Dust Grain Growth in a Protoplanetary Disk: Effects of Location on Charge and Size

Will Barnes, Lorin S. Matthews, Truell W. Hyde *Member, IEEE*

***Abstract*—In this paper, we investigate deviations in grain growth and charge due to the location of the dust within a protoplanetary disk. Using a particle-particle, particle-cluster, and cluster-cluster coagulation model as well as an aggregate charging model, we examine the formation and charging of dust aggregates over a range of radii and elevations. We show the relationship between grain charge and number of monomers as well as aggregate shape. The results show that, for all of the locations considered, grain charging was not large enough to significantly impact grain size and growth. Some possible improvements and topics for future work are discussed as well.**

***Index Terms*—accretion disks, dust coagulation, planets: formation, protoplanetary disks**

I. Introduction

PROTOPLANETARY disks, the sites of planet formation, have their origins in the processes behind the birth of stars. Cold, dense molecular cloud cores, made up of dust and gas, within nebulae collapse due to gravitational instabilities. Young stellar objects (YSOs) form a the center of the core where the gas and dust are the most dense. During the collapse, the mass of gas and dust in the cloud transitions from being distributed over parsec (pc) scales to being confined to astronomical unit (AU) scales. Redistribution and conservation of angular momentum leads to the remaining gas and dust forming a disk-shaped structure which we refer to as the accretion disk. This disk then evolves into a more tenuous protoplanetary disk (PPD) [1]. It is in this structure that the first stages of planet formation begin.

The growth of micrometer- and submicrometer-sized dust particles into kilometer-sized planetesimals is the initial stage of planet formation with the first step being the coagulation of initially submicrometer-sized particles into highly porous fractal aggregates [7]. The collisions and and sticking of dust monomers (single spherical particles) and aggregates (two or more monomers stuck together) is a complex process that requires an in-depth of knowledge of both the properties of the dust grains as well as their environment. In a protoplanetary disk, a weakly-ionized gas or plasma is the dominant component. Dust grains in the disk couple to the gas and thus their motions are determined primarily by Brownian motion and turbulence [5]. Both of these phenomena will be discussed later on. However, because the gas is ionized, there is another effect that can be taken into consideration: dust grain charging.

Although dust aggregation in planet formation is well-recognized, few have explored the role of charging in dust aggregation within the context of the PPD [6]. Because the gas is (weakly) ionized, a certain number of electrons and ions are present in the disk. These plasma particles can collide with the dust, causing it to charge negatively (electron collsions) or positively (ion collisions). See Fig. 1 for an illustration of this. This ionization also gives rise to a phenomenon known as a magnetorotational instability (MRI) which is now thought to be one of the main causes of turbulence in the disk and thus a central component of grain growth [5], [6]. Additionally, [7] show that charging of dust grains has a significant impact on size distribution within the protoplanetary disk and can even lead to the formation of a so-called “frozen zone” within the disk. [5] also show that the charge on an aggregate affects its size, mass, and “fluffiness,” characterized by the compactness factor ϕ_σ. Thus, charging is clearly a key factor in grain growth within a PPD.

In this paper, we investigate aggregation within the PPD as affected by grain charging. Partially utilizing the coordinates specified by [12], we calculate initial conditions for elevations of Z =

This material is based upon work supported by the National Science Foundation under Grant No. 0847127.

W. Barnes, L. S. Matthews, and T. W. Hyde are with the Center for Astrophysics, Space Physics, and Engineering Research, Baylor University, Waco, TX 76798 USA (e-mail: Will_Barnes@Baylor.edu; Lorin_Matthews@Baylor.edu; Truell_Hyde@Baylor.edu)

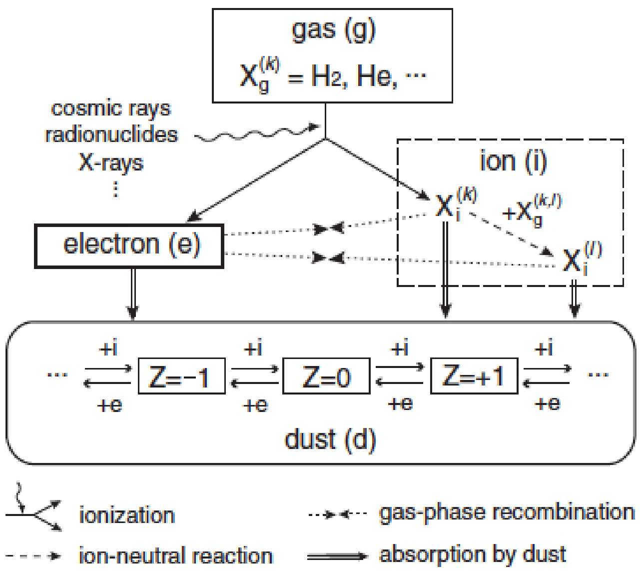

Fig. 1. Fig.1 from [6]; this schematic shows the ionization of the gas by cosmic rays, X-rays, and radionuclides as well as the subsequent absorption of charged particles by the dust grains. As shown by the dotted arrows, ions and electrons can also be removed by gas-phase recombination.

$0.8H, 0.9H, H$ AU at radial distances $R = 2, 5$ AU, where H is the vertical scale height (defined in section II-C). For each of these locations in the PPD, using a numerical model written in MATLAB, we construct aggregates through particle-particle, particle-cluster, and cluster-cluster aggregation (PPA, PCA, and CCA, respectively). We then show the impact of dust grain charging on aggregation and compare the presence of this effect between the different locations in the disk.

II. Methods

A. Building Dust Aggregates

The main collection of code we used in our simulations is known as `Aggregate_Builder`. This set of code allows us to construct aggregates for various locations within the disk through PPA, PCA, and CCA. These three levels of construction or ”generations” are described in detail in section 2.3 of [5]. The code comprising `Aggregate_Builder` is based on codes for N-body simulations by [9], [10]. However, our code examines only pairwise particle interactions and has been extended to include the effects of charged particles as well as magnetic fields [5].

To begin with, a particle, either a monomer or an aggregate (depending on whether this is PPA, PCA, or CCA) is placed at the origin. Then, a monomer (or an aggregate) is shot towards the target particle from a randomly selected direction. All particle collisions occur in the center-of-mass (COM) reference frame of the target particle. The monopole and dipole terms of each particle are used to calculate the electric fields of each particle. The electrostatic force due to said fields is then taken into account when calculating the accelerations of each particle. Additionally the dipole moment of each particle $\vec{p_i}$ can also interact with the electric field of the opposite particle $\vec{E_j}$ to produce a torque about the COM of the target particle,

$$\vec{\Gamma_i} = \vec{p_i} \times \vec{E_j}, \tag{1}$$

[4]. The motion resulting from these torques is governed by Euler's equations,

$$\lambda_1\dot{\omega}_1 - (\lambda_2 - \lambda_3)\omega_2\omega_3 = \Gamma_1, \tag{2}$$
$$\lambda_2\dot{\omega}_2 - (\lambda_3 - \lambda_1)\omega_3\omega_1 = \Gamma_2, \tag{3}$$
$$\lambda_3\dot{\omega}_3 - (\lambda_1 - \lambda_2)\omega_1\omega_2 = \Gamma_3. \tag{4}$$

Here, λ_i is the principal moment of inertia and ω_i is the angular velocity with respect to the body axes.

A fifth-order Runge-Kutta method is utilized to determined the resulting position, velocity and orientation of the target grain. The statistics are updated appropriately in the data structure called `AGG`. The information for the impinging grain is stored in `NEW`. Updates are made regardless of whether there is a collision or missed collision. Further details regarding this algorithim can be found in [4].

B. Charging Dust Aggregates

To simulate the charging of dust grains within the PPD, we employ an aggregate charging code that relies on Orbital Motion Limited theory and the line of sight approximation, appropriately dubbed `OML_LOS`. This section will give a brief overview of the calculations done using the algorithim and the physical reasoning behind them.

Because the dust grain is bathed in a plasma within the PPD environment, ions and electrons continuously bombard the grain, with electrons colliding more frequently. The current density due to an incoming particle (an electron or ion) is given by,

$$J_\alpha(t) = n_\alpha q_\alpha \iiint f_\alpha(v_\alpha) v_\alpha \cos(\theta)\, d^3\vec{v_\alpha}, \tag{5}$$

$$J_\alpha(t) = n_\alpha q_\alpha \int_{v_m(t)}^{\infty} f_\alpha(v_\alpha) v_\alpha^3\, dv_\alpha \times \iint \cos(\theta)\, d\Omega, \tag{6}$$

[5]. Here, n_α is the plasma density far from the particle, q_α is the charge on the impinging electron (or ion), f_α is the velocity distribution function, $v_\alpha \cos(\theta)$ is the velocity component of the electron (ion) perpendicular to the surface, and $d\Omega$ is the solid angle.

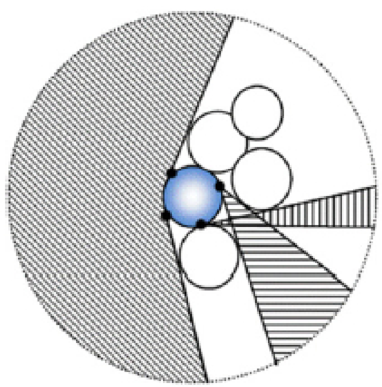

Fig. 2. Fig.1 from [5]; this is an illustration of the line of sight (LOS) approximation. Because of the structure of the aggregate, not all directions are open to allow for an impinging electron (or ion) to travel along them. The LOS approximation helps determine which lines of sight are blocked (those in the white space) and which are open (those in the shaded space).

For a sphere with lines of sight that are completely unblocked, the solid angle, $d\Omega$, is trivial. However, consider the illustration in Fig. 2. For the shaded sphere with the four test points, lines of sight in the shaded area are open while those in the white area are blocked by other monomers. $d\Omega$ then must be computed only over these open lines of sight. To determine which are blocked or unblocked, the surface of the monomer is divided up into many small patches of equal area. Vectors are constructed that go from the center of the monomer through surface patch. If these "lines of sight" intersect with any other monomer in the aggregate, the direction is considered blocked. Otherwise, it is unblocked. This determination then allows for the calculation of the LOS_factor, the numerical approximation of the solid-angle integral [5].

In [5], it can be seen that the charge is nearly linearly proportional to the equivalent radius. For aggregates with $N \geq 200$, we use a charging method that involves linear fits of the charge and equivalent radius data. This allows for a drastic reduction in computational time as individual aggregates do not need to be charged in `OML_LOS`.

C. Initial Conditions

Since we are considering multiple locations in the disk as sites for potential aggregate growth, we must take into account a range of initial conditions. We assume a Maxwellian distrubution for the plasma species [3], [5]. The temperature, T, assumed to be constant in Z, and the gas density, ρ_g, were estimated and calculated from Figs. 1a and 1b of [13] and Eqs. 44 and 45 of [6]. Fractional ionization (X_e) estimations were made based on Fig. 2 of [11]. For all of the elevations at $R = 5$ AU we considered, we assumed $X_e = 10^{-10}$. Position-dependent estimates of the electron depletion, n_e/n_i, and average number of electrons per monomer were made from Figs. 4a and 4b of [5]. These values are used to determine the ion density and average monomer potential, respectively.

The size of the dust within the PPD is assumed to be distributed according to the Mathis-Rumpl-Nordsieck (MRN) distribution for dust in the interstellar medium,

$$n(a_0) \propto a_0^\alpha da_0, \tag{7}$$

where $\alpha = -3.5$ [2]. In all of our simulations, monomers are spherical particles with radii in the range of $0.5\mu m \leq a_0 \leq 10\mu m$, with an average radius of $\langle a_0 \rangle = 0.83\mu m$. Monomers were assumed to be composed of silicates with a mass density of $\rho_m = 2.5$ kg/m^3. This material composition is relevant at these locations in the disk, but is location dependent.

Gas in many astrophysical environments is subject to turbulence and the PPD is no exception [8]. As previously stated, an ionized gas can give rise to a MRI, thought to be one of the main causes of turbulence in the disk. Additionally, [5] make the assumption that turbulence is the main contributor to the relative velocity between particles in the PPD. Concerning, this relative velocity, for tightly coupled particles in the small particle regime, [8] give the expression,

$$\Delta V_{12} = \sqrt{\frac{3}{2}}(t_1 - t_2)\frac{V_\eta}{t_\eta}, \tag{8}$$

where $t_{1,2}$ are the stopping times of the first and second particle, $V_\eta = \mathrm{Re}^{-1/4} V_L$ is the velocity of the smallest eddy, and $t_\eta = \mathrm{Re}^{-1/2} t_L$ is the turnover time of the smallest eddy [7]. Here, $\mathrm{Re} = \alpha c_g H/\nu_m$ is the Reynolds number as given by [5] where c_g is the sound speed of the gas, $H = c_g/\Omega_K$ is the vertical scale height, and $\nu_m = \sqrt{2/\pi} m_g c_g/\rho_g \sigma_{coll}$, given by [7], is the molecular viscosity. Following [5], we choose $\alpha = 0.01$, where α is a parameter describing the strength of the turbulence in the disk. $V_L = \sqrt{\alpha} c_g$ and $t_L = \Omega_K^{-1}$ are the velocity and turnover time of the largest eddy, respectively, as defined by [7].

As mentioned previously, the disk is assumed to be vertically isothermal. However, as we move radially outward in the disk, T decreases. Thus, since $c_g := c_g(T)$, the sound speed of the gas also has a radial dependence. Additionally, $\Omega_K := \Omega_K(R)$ and $\rho_g := \rho_g(R, Z)$. As a result, nearly all of the initial parameters discussed have an R and/or Z dependence.

III. Results

Following the completion of our generation one aggregates for $R = 2$ AU conditions, the aggregates were examined to ensure ample charge was accumulating on them. The average number of electrons ($\langle Z_D \rangle$) versus the number of monomers (N) per aggregate is shown in Fig. 3 for six different vertical coordinates. The three lowest spots ($Z/H = 0.4, 0.6, 0.7$) show essentially no charge for first generation aggregates. In contrast, the three highest spots ($Z/H = 0.8, 0.9, 1.0$) show up to six electrons on the smallest monomers and a somewhat linear increase in $\langle Z_D \rangle$ as N increases. This motivated further examination of the three highest locations in our disk at both $R = 2$ AU and $R = 5$ AU.

As one would expect, mass increases as the number of monomers in our aggregate increases. This relationship is shown in Figs. 4a and 4b. The fit lines for our three heights nearly all overlap for aggregates at $R = 2$ AU. This is even more true at $R = 5$ AU, hence the offset of our linear fits to our log-log plots.

We are most interested in the charge on our aggregates and how this affects growth and size.

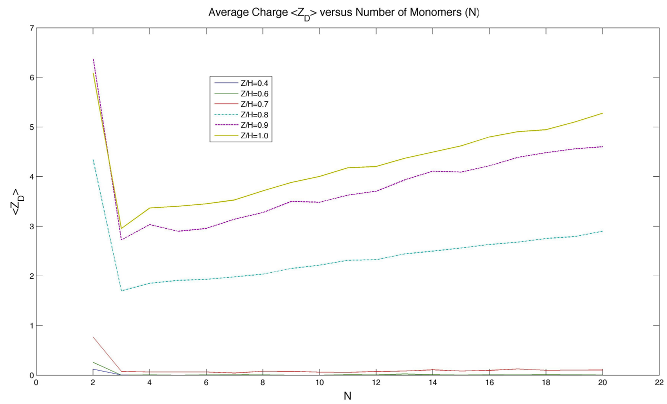

Fig. 3. Average charge per aggregate versus number of monomers. All aggregates are generation one aggregates with $N \leq 20$ monomers. Three lower locations in the disk are shown here as well.

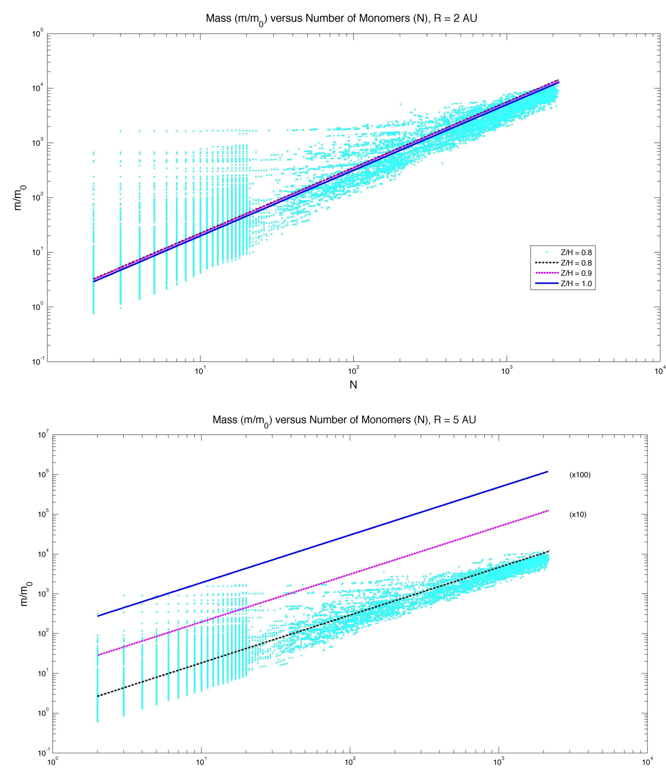

Fig. 4. Log-log plot of the Mass scaled by the average mass ($m_0 = 5.9877 \times 10^{-15}$) versus number of monomers for (a)$R = 2$ AU and (b)$R = 5$ AU with three different Z/H values shown for each. The trendlines in (b) for 0.9 and 1.0 are offset by 10 and 100 respectively. Only the linear fits are shown for $Z/H = 0.9, 1.0$ for aesthetic purposes.

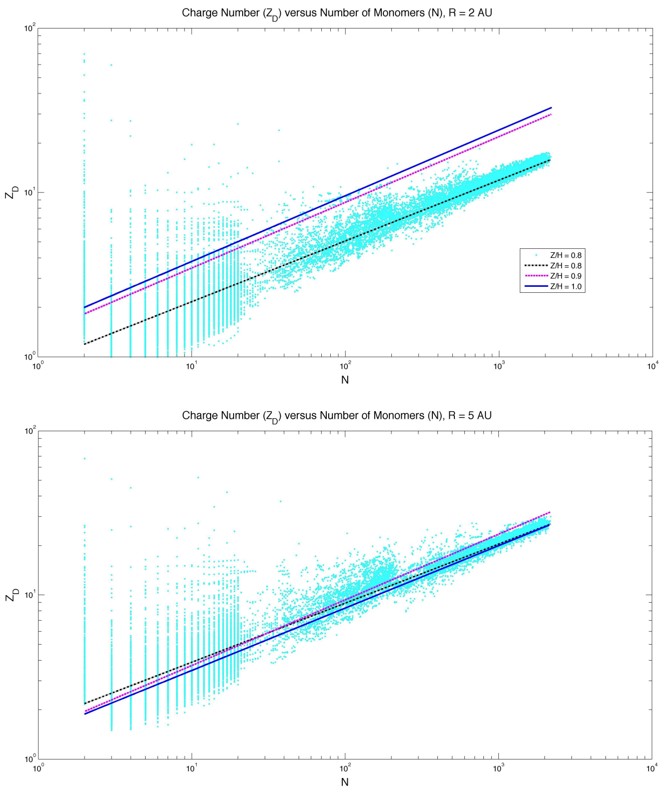

Fig. 5. Log-log plot of charge number versus number of monomers for (a)$R = 2$ AU and (b)$R = 5$ AU with three different Z/H values shown for each. Only the linear fits are shown for $Z/H = 0.9, 1.0$ for aesthetic purposes.

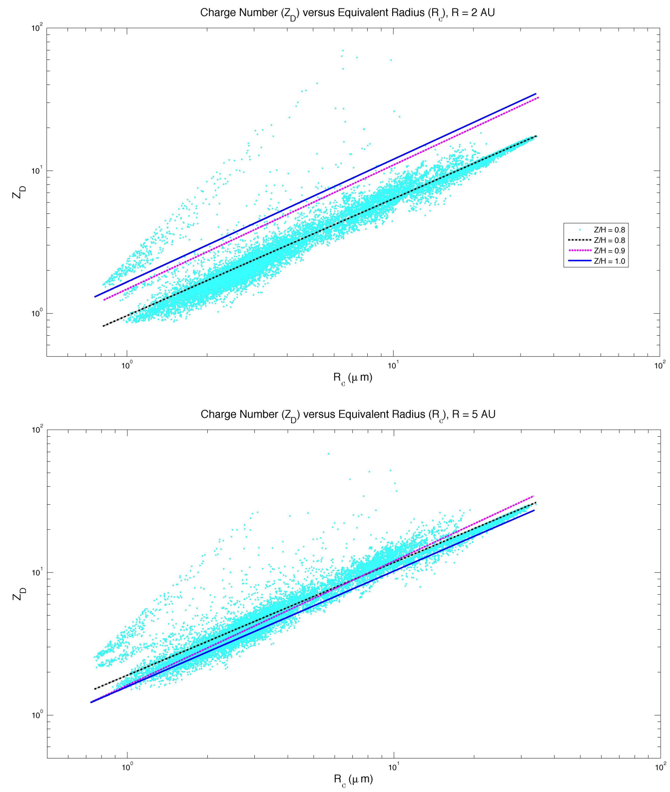

Fig. 6. Log-log plot of the charge number versus the equivalent radius for (a)$R = 2$ AU and (b)$R = 5$ AU with three different Z/H values shown for each. Only the linear fits are shown for $Z/H = 0.9, 1.0$ for aesthetic purposes.

Figs. 5a and 5b show the relationship between Z_D and N. First generation aggregates at all heights and both radii show a very large spread in Z_D. Aggregates with $N > 20$ have a narrower distribution of charges. Aggregates at all Z/H values at $R = 5$ have greater charge than those grains at $Z/H = 0.8$ and $R = 2$ AU. However, as can be seen by the fit lines for $Z/H = 0.9, 1.0$ in 5a, the difference between higher and lower elevations with respect to Z_D is greater. This data corresponds well with the values of $\langle Z_D \rangle$ for first generation aggregates as seen in Fig. 3.

Following [5], we examine the relationship between Z_D and the equivalent radius, R_σ, a quantity related to the compactness factor, ϕ_σ, which characterizes the “fluffiness” of the aggregate. Considering this relationship allows us to see how the amount of charge on an aggregate affects its morphology or shape. As in [5], we find a fairly narrow, linear relationship in our log-log plots of Z_D and N. This is true for all six of our locations within the disk. Again, as in Figs. 5a and 5b, higher charges are seen for $Z/H = 0.8$ at $R = 5$ AU, but larger differences in Z_D exist with respect to Z/H at $R = 2$ AU.

IV. Discussion and Conclusions

Concerning our preliminary results in Fig. 3, it is not surprising that our lower disk heights yield lower values for Z/H. As dust grains coagulate and increase in mass, they settle toward the increasingly more dense midplane. This high dust density causes a high opacity in this region, effectively shielding the gas in the disk from X-ray and cosmic ray radiation. As a result, these locations are subject to much lower fractional ionization values. A greater number of electrons combined with fewer free electrons results in few electrons per aggregate.

In [5], the location $R = 1$ AU, $Z/H = 0.5$ is considered for several different values of the electron depletion. In their Fig. 10a, it can be seen that even for the smallest electron number density, charges of $Z_D \approx 10^3$ are acheived for the largest, most fluffy aggregates. As can be seen from Figs. 5 and 6, we see charges on our grains that are markedly lower for approximately equivalent N and R_σ. This is most likely due to the significantly lower temperatures we consider, $T = 300, 175$ K for $R = 2, 5$ AU, respectively, as compared to $T = 900$ K for $R = 1$ AU used by [5].

We conclude that there is a correlation between Z_D and N as well as Z_D and R_σ, a relationship that is also shown in [5]. However, we do not observe a significant amount of charge on even our largest grains ($N \approx 2000$). We believe that these minute charges are not large enough to signicantly impact dust grain growth in the PPD. Improving the validity of X_e estimations and calculations as well as considering higher Z/H values will, we believe, lead to significantly larger charge on grains at a variety of locations within the PPD. It is certainly possible that at the locations considered, conditions are not adequate for grain charging. Much future work is needed.

V. Future Work

As stated in section II-C, the values used for X_e were estimates, rather than direct calculations. We believe these estimations to be a source of error in our simulations. Methods for calculating X_e are given in [7] and [11] and are possible candidates for determining this value. We believe that more accurate values for the fractional ionization will allow for better differentiation between charging at different locations in the disk. Additionally, examination of higher elevations in the disk is necessary. Currently, our chosen vertical coordinates yield very little charge on our aggregates. This may be due to shielding from X-ray and cosmic ray radiation sources as well as a high dust density that leads to fewer electrons per grain.

Low disk temperatures are another possible explanation for the low charge numbers on our largest dust grains. Considering a PPD at an earlier evolutionary stage would allow for higher disk temperatures as less disk material has been depleted by radiation and accretion onto the star.

The elemental composition of the gas is another uncertainty. Here, we assumed a hydrogen plasma, but is important to note that other elements of varying abundances are also present within the disk, with said abundances depending on the location within the disk [11].

Acknowledgment

We thank the Center for Astrophysics, Space Physics and Engineering Research (CASPER), particularly the members of the Astrophysics and Space Science Theory Group, as well as the Department of Physics, Baylor University. Also, we thank Victor Land for his helpful input on this topic throughout the summer. Additionally, we extend our thanks to all of the 2012 CASPER Research Experience for Undergraduates/Teachers (REU/RET) Fellows as well as the National Science Foundation for funding this research.

References

[1] Apai, D. and D. S. Lauretta 2010. Planet Formation and Protoplanetary Dust. *Protoplanetary Dust*, 1-26.
[2] Mathis, J. S., W. Rumpl, and K. H. Nordsieck 1977. The Size Distribution of Interstellar Grains. *Astrophys. J.* **217**, 425-433.
[3] Matthews, L. S. and T. W. Hyde 2008. Charging and Growth of Fractal Dust Grains. *IEEE Trans. Plasma Sci.* **36**, 310-314.
[4] Matthews, L. S., R. L. Hayes, M. S. Freed, and T. W. Hyde 2007. Formation of Cosmic Dust Bunnies. *IEEE Trans. Plasma Sci.* **35**, 260-265.
[5] Matthews, L. S., V. Land, and T. W. Hyde 2012. Charging and Coagulation of Dust in Protoplanetary Plasma Environments. *Astrophys. J.* **744**, 1-12.
[6] Okuzumi, S. 2009. Electric Charging of Dust Aggregates and Its Effect on Dust Coagulation in Protoplanetary Disks. *Astrophys. J.* **698**, 1122-1135.
[7] Okuzumi, S., H. Tanaka, T. Takeuchi, and M. Sakagami 2011. Electrostatic Barrier Against Dust Growth in Protoplanetary Disks. II. Measuring the Size of the "Frozen" Zone. *Astrophys. J.* **731**, 1-14.
[8] Ormel, C. W. and J. N. Cuzzi 2007. Closed-form Expressions for Particle Relative Velocities Induced by Turbulence. *Astron. Astrophys.* **466**, 413-420.
[9] Richardson, D. C. 1993. A New Tree Code Method for Simulation of Planetesimal Dynamics. *Mon. Not. R. Astron. Soc.* **261**, 396-414.
[10] Richardson, D. C. 1995. A Self-Consistent Numerical Treatment of Fractal Aggregate Dynamics. *Icarus* **115**, 320-335.
[11] Semenov, D., D. Wiebe, and Th. Henning 2004. Reduction of Chemical Networks. II. Analysis of the Fractional Ionization in Protoplanetary Discs. *Astron. Astrophys.* **417**, 93-106.
[12] Weidenschilling, S. J. 1984. Evolution of Grains in a Turbulent Solar Nebula. *Icarus* **60**, 553-567.
[13] Willacy, K., H. H. Klahr, T. J. Millar, and Th. Henning 1998. Gas and Grain Chemistry in a Protoplanetary Disk. *Astron. Astrophys.* **338**, 995-1005.
[14] Williams, J. P. and L. A. Cieza 2011. Protoplanetary Disks and Their Evolution. *Ann. Rev. Astr. Astrophys.* **49**, 1-65.

Will Barnes is currently working toward a B.S. degree in astrophysics at Baylor University, Waco, Texas.

Lorin S. Matthews is an Assistant Professor with the Physics Department, Baylor University as well as the Associate Director of the Center for Astrophysics, Space Physics, and Engineering Research (CASPER).

Truell W. Hyde is a Professor of Physics and the Vice Provost for Research, Baylor University. He is also the Director of CASPER.